

Cooperative Jahn-Teller transition and resonant x-ray scattering in thin film LaMnO₃

J. H. Song, J. H. Park, K. -B. Lee, and Y. H. Jeong

*Department of Physics and electron Spin Science Center,
Pohang University of Science and Technology,
Pohang, Kyungbuk, 790-784, S. Korea*

Abstract

Epitaxial thin films of stoichiometric LaMnO₃ were grown on SrTiO₃(110) substrates using the pulsed laser deposition technique. From the high resolution x-ray diffraction measurements, the lattice parameters were determined as a function of temperature and the cooperative Jahn-Teller transition was found to occur at $T_{JT}=573.0$ K. Also measured was resonant x-ray scattering intensity of the orthorhombic (100) peak of LaMnO₃ near the Mn K edge from low temperatures to above T_{JT} . We demonstrate that the integrated intensity of the (100) peak is proportional to the 3/2 power of the orthorhombic strain at all temperatures, and thus provide an experimental evidence that the resonant scattering near the Mn K edge in LaMnO₃ is largely due to the Jahn-Teller effect.

PACS numbers: 75.30.Vn, 78.70.Ck, 61.10.Dp, 71.90.+q

Orbital degrees of freedom representing anisotropically shaped $3d$ orbitals are of importance for understanding magnetic, structural, and electronic properties of transition metal oxides [1]. For instance, superexchange interactions between electrons occupying neighboring transition metals are very sensitive to the orientation of occupied $3d$ orbitals [2, 3, 4], and the magnetic properties are strongly coupled to the orbital degrees of freedom. Also important regarding orbital degeneracy is the well-known Jahn-Teller (JT) distortion [5]; moreover, these local distortions may even behave cooperatively leading to a structural transition. Electronic transport properties of transition metal oxides, of course, is also strongly affected by the relative orientation of occupied orbitals on neighboring ions; the double exchange mechanism is a good example [6].

Despite a recognized role that the orbital degrees of freedom play in transition metal oxides, securing a *direct* experimental probe for orbital order has long been problematic; however, Murakami *et al.* proposed in a recent series of experimental works that resonant x-ray scattering (RXS) is a direct probe of orbital order [7]. The RXS signal near the Mn K edge in perovskite manganite samples was interpreted to be sensitive to the status of $3d$ electrons and their orbital ordering. Since the transition was supposed to be a dipolar one from $1s$ to $4p$, the origin of the sensitivity of RXS to $3d$ orbital order became controversial. Murakami *et al.* originally interpreted the RXS data based on the localized $4p$ states and their subsequent splitting due to the interaction with $3d$ orbitals. Ishihara *et al.* then specified the interaction to be the Coulomb repulsion between $3d$ and $4p$ states [8]. However, this $3d$ orbital ordering interpretation was immediately questioned by Elfmov *et al.* [9]; they used band calculations to show that the JT effect (JTE) is a major player in RXS. (JTE is used here to include both local JT distortion of MnO_6 octahedra and their subsequent cooperative ordering.) Indeed it is expected that $4p$ states form a broad band in solids, and the $3d - 4p$ direct Coulomb interactions in the band would not be as strong as in localized states; a number of band calculations for LaMnO_3 now assert that Mn $4p$ states strongly hybridize with the neighboring O orbitals and the RXS intensity and its polarization dependence are determined mostly by this Mn–O hybridization and thus by JTE, rather than by the orbital order of the $3d$ states [9, 10, 11, 12].

LaMnO_3 , a parent material of colossal magnetoresistance manganese oxides, has been at the center of orbital physics from the beginning, that is, Goodenough invoked orbital order to account for the A-type antiferromagnetic order in LaMnO_3 [13]. Thus LaMnO_3 appears

to be a good system for the observation of orbital ordering, and Murakami *et al.* measured RXS from a single crystalline LaMnO₃ to investigate orbital ordering. However, this system undergoes a concomitant cooperative JT transition [14], and the characteristics of RXS can also be explained in terms of the JTE as noted above. In the present study we attempted to address this point experimentally by focusing specifically on the relationship between the lattice distortion from the JTE and the RXS intensity. We demonstrate that the RXS signal is in proportion to the 3/2 power of the lattice orthorhombicity in LaMnO₃ at all temperatures; this result provides an evidence that the long range order of JT distorted MnO₆ octahedra and the associated band effect are indeed a dominant factor in RXS.

The samples used in the present experiment were *epitaxial* thin films of LaMnO₃ deposited on SrTiO₃ substrates. Using a LaMnO₃ bulk pellet as a target, thin films of thickness approximately 2000 Å were deposited on SrTiO₃(110) single crystal substrates by the pulsed laser deposition method [15]. The substrates, of typical dimension 5 mm x 5 mm, were annealed for approximately 10 hours at 1000°C in oxygen environment to obtain atomically flat surfaces, and then films were deposited on the substrates at 800°C and 180 mTorr of oxygen pressure. Since as-grown LaMnO₃ films may contain excessive oxygen, post-deposition thermal treatment was done at about 950°C in flowing argon. The post-annealing procedure also improved the structural quality of the films; the mosaic width (FWHM) of the (200) reflection was about 0.2°. X-ray scattering measurements were performed on the beamline 3C2 at the Pohang Light Source. The incident beam is focused by a bent mirror and is monochromatized by a Si(111) double crystal. The energy was calibrated using a manganese foil and the resolution was about 2 eV.

At this point, remarks on the choice of the substrate and film orientation are in order. It is known from the neutron study of bulk samples that LaMnO₃ below the structural transition temperature (ca. 750 K) has an orthorhombic *Pbnm* crystal structure, and the orthorhombic unit cell volume is $\sqrt{2} \times \sqrt{2} \times 2$ times as large as that of the perovskite cubic cell [14]. We designate these directions and lattice parameters as *a*, *b*, and *c*, and the parameters satisfy the relation, $a > b > c/\sqrt{2}$. (The Miller indices used for LaMnO₃ in this paper are orthorhombic ones.) Neutron powder diffraction also indicated that the JT distortion of MnO₆ octahedra accompanies the structural change from a high *T* pseudocubic phase to a low *T* orthorhombic one, and thus the transition is a cooperative JT type. In the orthorhombic phase, antiferro-type 3*d* orbital ordering and concomitant ordering of the

distorted octahedra occur in the *ab*-plane [13]. Thus in order to investigate these ordered states in the *ab*-plane, one must probe the normally forbidden ($h00$) or ($0k0$) peaks with odd h and k . From this consideration, it is preferred to have *a*- or *b*-direction as a surface normal; one should deposit LaMnO₃ on the (110) surface of a cubic substrate, rather than on the usual (100) surface. Then the surface-normal *cubic* [110] direction of the substrate would corresponds to the *orthorhombic* [100] direction of the film. SrTiO₃ was chosen as substrate, because its lattice constant (3.905 Å) closely matches the lattice spacing of LaMnO₃.

Fig. 1 is the contour plot of x-ray diffraction data obtained at 6.529 keV of photon energy. It shows the reciprocal space mapping in the vicinity of the substrate (200) reflection at two temperatures. It is seen from Fig. 1(a) that the (220) peak of the LaMnO₃ film (in orthorhombic notation) is in registry with the cubic (200) peak of SrTiO₃ at $T = 573.2$ K. The lattice spacings of the LaMnO₃ film at this temperature is nearly equal (3.928Å, 3.917Å, and 3.912Å), and the system is pseudocubic. At room temperature, on the other hand, we find two diffraction peaks, instead of one, from the film as plotted in Fig. 1(b). This indicates that one has two domains of different orientations, denoted as *A* and *B* domains (corresponding to F_a and F_b in the figure, respectively). Clearly this is the result of the effort of the system which tried to reduce the strain energy as much as possible when the system underwent the transition from a pseudocubic to orthorhombic phase. Domain formation is often found in a thin film which undergoes a structural change [16]. The difference between the two domains lies in their relative orientation, and we focus on the *A* domain only. The lattice constants and orientation of the *A* domain were determined from in-plane and out-of-plane reflections. The lattice constants in terms of the cubic cell parameters were 3.983Å, 3.912Å, and 3.866Å; the domain had its *c*-axis (with the shortest lattice spacing) parallel to [001] in the substrate surface, and the *a*-axis parallel to the substrate surface normal [110]. Thus the *ab*-planes of the *A* domain stood perpendicular to the substrate surface.

In order to characterize the phase transition, we carried out x-ray diffraction measurements as a function of temperature. In Fig. 2 plotted are *a* and *b* lattice constants and the orthorhombic strain ($a - b$) against temperature, and it is seen that the structural transition occurs at $T_{JT} = 573.0$ K. This transition, of course, corresponds to the cooperative JT one which occurred at 750 K in bulk ceramic samples. This reduction in transition temperature is not at all surprising, considering the fact that a thin film is generally under biaxial stress due to lattice mismatch with the substrate and/or differential thermal expansion between

the film and substrate. The fact that a single crystal bulk sample shows the transition at 780 K [7], 30 K higher than the ceramic case, clearly illustrates the role of stress in determining the transition temperature. If the lattice constants of the epitaxial film at room temperature (given above) are compared with those of a bulk sample at the same temperature (4.060Å, 3.912Å, and 3.834Å) [17], it is recognized that the orthorhombicity of the film is much less than that of the bulk. Thus the underlying SrTiO₃ substrate has the effect on the film of suppressing the JT transition. The decrease of the transition temperature in thin film case is also in accord with a recent pressure study of LaMnO₃ that the coherent JT distortion is reduced with increasing pressure [18].

Having characterized the cooperative JT transition, we turn to the discussion of RXS near the Mn K edge; here we focus on the structurally forbidden (100) peak of LaMnO₃. Note that the momentum transfer direction for this peak of the *A* domain is the surface normal. Fig. 3 displays the characteristics of absorption and RXS obtained at 15.5 K from the (100) peak of the *A* domain. Fig. 3(a) is the plot of fluorescence data of Mn³⁺ K absorption as a function of incident photon energy. The shape of the curve including the splitting into two peaks matches the 4p total density of states from the band calculation, indicating the dipolar nature of the process (1s → 4p) [9]. The (100) peak exhibits a resonance-type enhancement in the integrated intensity as a function of energy and reaches a maximum at 6.555 keV as illustrated in Fig. 3(b). Since the incident synchrotron beam is σ -polarized (polarization perpendicular to the scattering plane) and RXS occurs via the $\sigma \rightarrow \pi$ channel, the RXS intensity should exhibit an oscillation in intensity as the *ab*-plane is rotated around the momentum transfer direction, i.e., the surface normal. Fig. 3(c) shows the results of the azimuthal scan measured at 6.555 keV of energy, revealing a sinusoidal variation with a two-fold symmetry. The integrated intensity plotted in the figure was normalized with the (200) fundamental charge reflection in order to correct for small variations due to the film shape. The azimuthal angle $\psi = 0^\circ$ was defined to be when the *ab*-plane is perpendicular to the scattering plane.

The features displayed in Fig. 3, resonance enhancement of the (100) peak and the two-fold symmetric nature of the integrated intensity as a function of azimuthal angle, follow from the fact that RXS is a second order process driven by the $\vec{A} \cdot \vec{p}$ term in the Hamiltonian; however, the same result can be derived either from the antiferro-type 3d orbital ordering or from the coherent ordering of the JT distorted MnO₆ octahedra in the *ab*-plane. The

essential ingredient in the theory is a breaking of the equivalence of two Mn sites (and the associated non-spherical $4p$ states) in the orthorhombic ab -plane, and this can be done by either of the two ways. Since these two types of order coexist in LaMnO_3 , it appears to be difficult to distinguish them as a origin of RXS. On the other hand, if one remembers that coherent ordering of local JT distortions brings about the structural transition, while orbital ordering itself seems to occur even without lattice distortion [19], then one is led to a conclusion: if the JTE is indeed the cause of RXS in LaMnO_3 , there *must* exist a certain relationship between the intensity of RXS and the degree of lattice distortion which would be proportional to the degree of local JT distortion. Thus, we focused our attention on revealing this relationship from the experimental data; the results are illustrated in Fig. 4.

Fig. 4(a) is the plot of the integrated intensity of the (100) peak as a function of temperature. The integrated intensity was measured at 6.555 keV of photon energy and the azimuthal angle was set at $\psi = 0^\circ$. The intensity disappears exactly at the same temperature T_{JT} where the orthorhombic strain does, as temperature is increased. Fig. 4(b) is the simultaneous plot of the integrated intensity and the normalized orthorhombic strain $e \equiv (a-b)/(a+b)$ as a function of temperature. Note that the vertical axis for the normalized strain is not e , but $e^{3/2}$. The fact that these two data sets can be superposed at all temperatures means that the RXS intensity is proportional to $e^{3/2}$; the inset, the plot of $e^{3/2}$ against the intensity, further highlights the proportional relationship. This simple relationship we exposed here, particularly the nontrivial exponent 3/2, must be able to distinguish the two proposed origins of RXS. In fact, the ab initio band calculation on LaMnO_3 by Benedetti *et al.* [12], which identified the JTE as the origin of RXS near the Mn K edge, predicted the proportional relationship between the integrated intensity and $e^{1.5}$. The present work then should be regarded as a definite experimental evidence that the resonant scattering near the Mn K edge in LaMnO_3 is due to the Jahn-Teller effect, rather than $3d$ orbital ordering.

One final remark on the relationship between the lattice orthorhombicity and the local JT distortion should be made, because one of these two aspects of LaMnO_3 does not automatically suggest the other. The orthorhombic symmetry may be induced from cubic perovskites just by a tilting of regular, not distorted, oxygen octahedra, e.g., CaTiO_3 [20]. In fact, even the high T phase of LaMnO_3 , where oxygen octahedra are regular, belongs to the $Pbnm$ class, not a cubic one [14]. These systems, however, are in sharp contrast to LaMnO_3 below T_{JT} , that is, their three lattice parameters are very close in size to each

other despite orthorhombicity, and they may be called *pseudocubic*. The significant lattice orthorhombicity in low T LaMnO₃ is the direct result of the local JT distortion: the long and short Mn-O bonds alternate in the *ab*-plane and contribute to a and b lattice parameters in different proportions due to the tilting of octahedra [21]. It is also noted that both the difference ($a - b$) of the lattice parameters and the difference in Mn-O bond lengths disappear simultaneously and continuously as T is increased toward T_{JT} . Evidently the lattice orthorhombicity and the degree of local JT distortion are proportional to each other.

In conclusion, we have demonstrated that the RXS intensity is proportional to the 3/2 power of the orthorhombic strain, and thereby showed that RXS near the Mn K edge is due to the JTE, rather than 3d orbital ordering.

We acknowledge the financial support from KOSEF via eSSC, the special fund of POSTECH, and the BK21. Experiments at the PLS were supported by MOST and POSCO. We thank Y.J. Park for technical assistance.

- [1] Y. Tokura and N. Nagaosa, Science **288**, 462 (2000).
- [2] J.B. Goodenough, *Magnetism and the Chemical Bonds* (Interscience, New York, 1963).
- [3] J. Kanamori, J. Phys. Chem. Solids **10**, 87 (1959).
- [4] K. I. Kugel and D. I. Khomskii, Sov. Phys. JETP **37**, 725 (1973).
- [5] H. A. Jahn and E. Teller, Proc. R. Soc. London, Ser. A **161**, 220 (1937).
- [6] C. Zener, Phys. Rev. **82**, 403 (1951).
- [7] Y. Murakami *et al.*, Phys. Rev. Lett. **81**, 582 (1998); Y. Murakami *et al.*, Phys. Rev. Lett. **80**, 1932 (1998).
- [8] S. Ishihara and S. Maekawa, Phys. Rev. Lett. **80**, 3799 (1999).
- [9] I. S. Elfimov *et al.*, Phys. Rev. Lett. **82**, 4264 (1999).
- [10] M. Benfatto *et al.*, Phys. Rev. Lett. **83**, 636 (1999).
- [11] M. Takahashi *et al.*, J. Phys. Soc. Jpn. **68**, 2530 (1999).
- [12] P. Benedetti *et al.*, Phys. Rev. B **63**, 060408(R) (2001).
- [13] J. B. Goodenough, Phys. Rev. **100**, 564 (1955).
- [14] J. Rodríguez-Carvajal *et al.*, Phys. Rev. B **57**, R3189 (1998).
- [15] T. Y. Koo *et al.*, Appl. Phys. Lett. **71**, 977 (1997).

- [16] B. S. Kwak *et al.*, Phys. Rev. B **49**, 14865 (1994).
- [17] J. Elemans *et al.*, J. Solid State Chem. **3**, 238 (1971).
- [18] I. Loa *et al.*, Phys. Rev. Lett. **87**, 125501 (2001).
- [19] Y. Endoh *et al.*, Phys. Rev. Lett. **82**, 4328 (1999).
- [20] S. Sasaki *et al.*, Acta Crystallogr. **43**, 1668 (1987).
- [21] D. N. Argyriou *et al.*, Phys. Rev. Lett. **76**, 3826 (1996).

Figure Captions

FIG. 1: The contour plot of x-ray diffraction data around the cubic (200) reflection of $\text{SrTiO}_3(110)$. q_{\perp} and q_{\parallel} are parallel to the [110] and [1 $\bar{1}$ 0] directions, respectively. (a) At 573.2 K, a single peak in registry with the substrate (200) peak is found from the film. Inset illustrates the momentum transfer of the substrate (200) peak. F and S denote the peaks from the film and substrate, respectively. (b) At room temperature, the two peaks (denoted as F_a and F_b) from two domains with different orientation are seen. Inset shows diffraction data along the surface-normal direction.

FIG. 2: The lattice constants a and b and the orthorhombic strain ($a - b$) as a function of temperature. The cooperative Jahn-Teller transition occurs at $T_{JT} = 573.0$ K. This transition temperature is somewhat low compared to 750 K of a bulk sample. This is due to the fact that the film is under biaxial stress. The lines are guide to the eye.

FIG. 3: X-ray absorption and resonant scattering near the Mn K edge. The data were obtained from the structurally forbidden (100) peak of the A domain at 15.5 K. (a) The fluorescence data is plotted as a function of photon energy. The shape of the curve matches well the $4p$ total density of states from the band calculation, indicating the $1s \rightarrow 4p$ process. (b) The integrated intensity for the (100) peak as a function of energy. The intensity exhibits a resonance-type enhancement around a maximum at 6.555 keV. (c) The integrated intensity of the (100) peak measured as a function of azimuthal angle is shown. The solid line represents a fit of the data to $\cos^2 \psi$.

FIG. 4: (a) Temperature dependence of the integrated intensity for the (100) peak. The intensity disappears at T_{JT} where the orthorhombic strain does, as temperature is increased. (b) The integrated intensity and the $3/2$ power of the normalized orthorhombic strain $e = (a - b)/(a + b)$ are plotted as a function of temperature simultaneously. The complete coincidence of these two data sets at all temperatures is further highlighted in the inset by plotting $e^{3/2}$ vs. intensity.

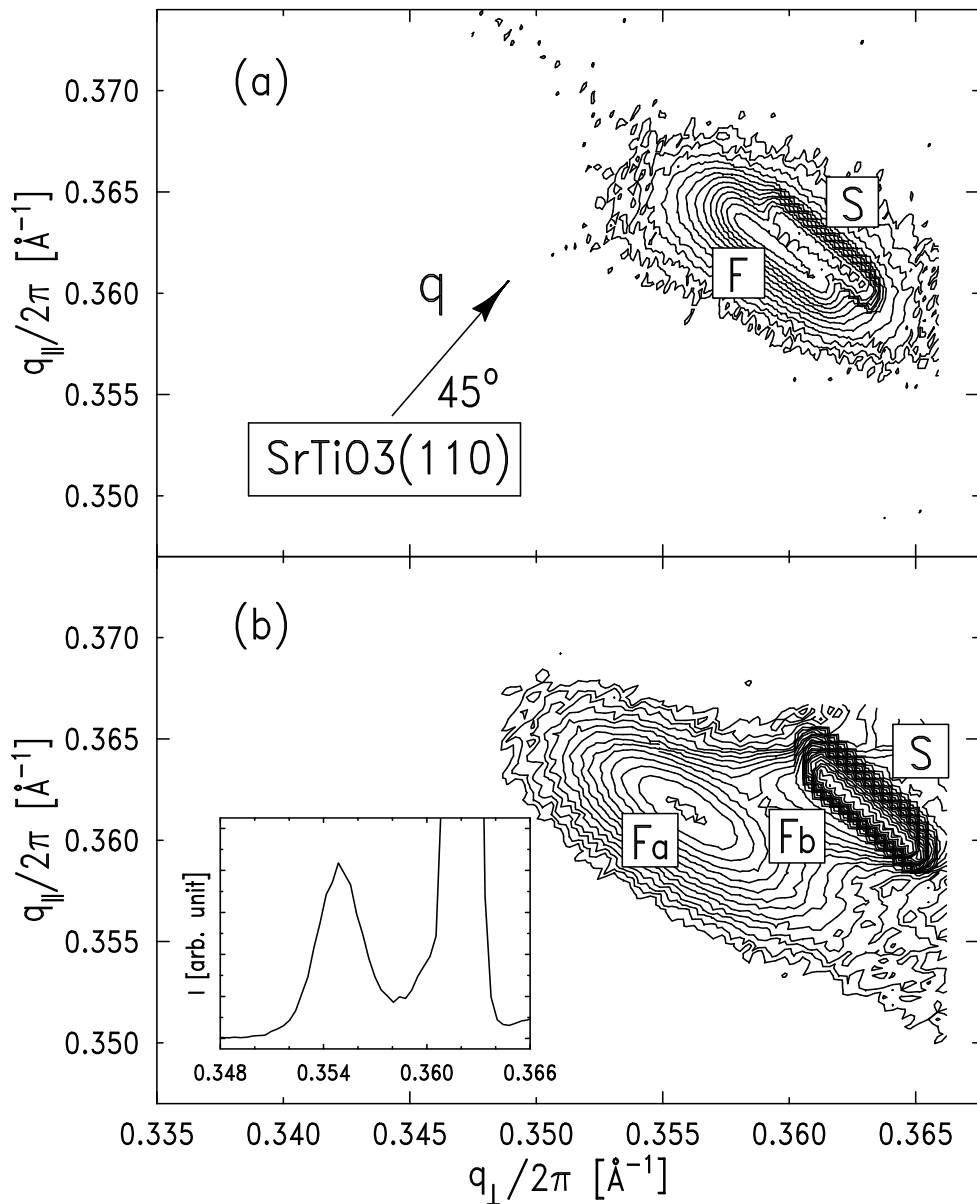


FIG. 1: Song et al.

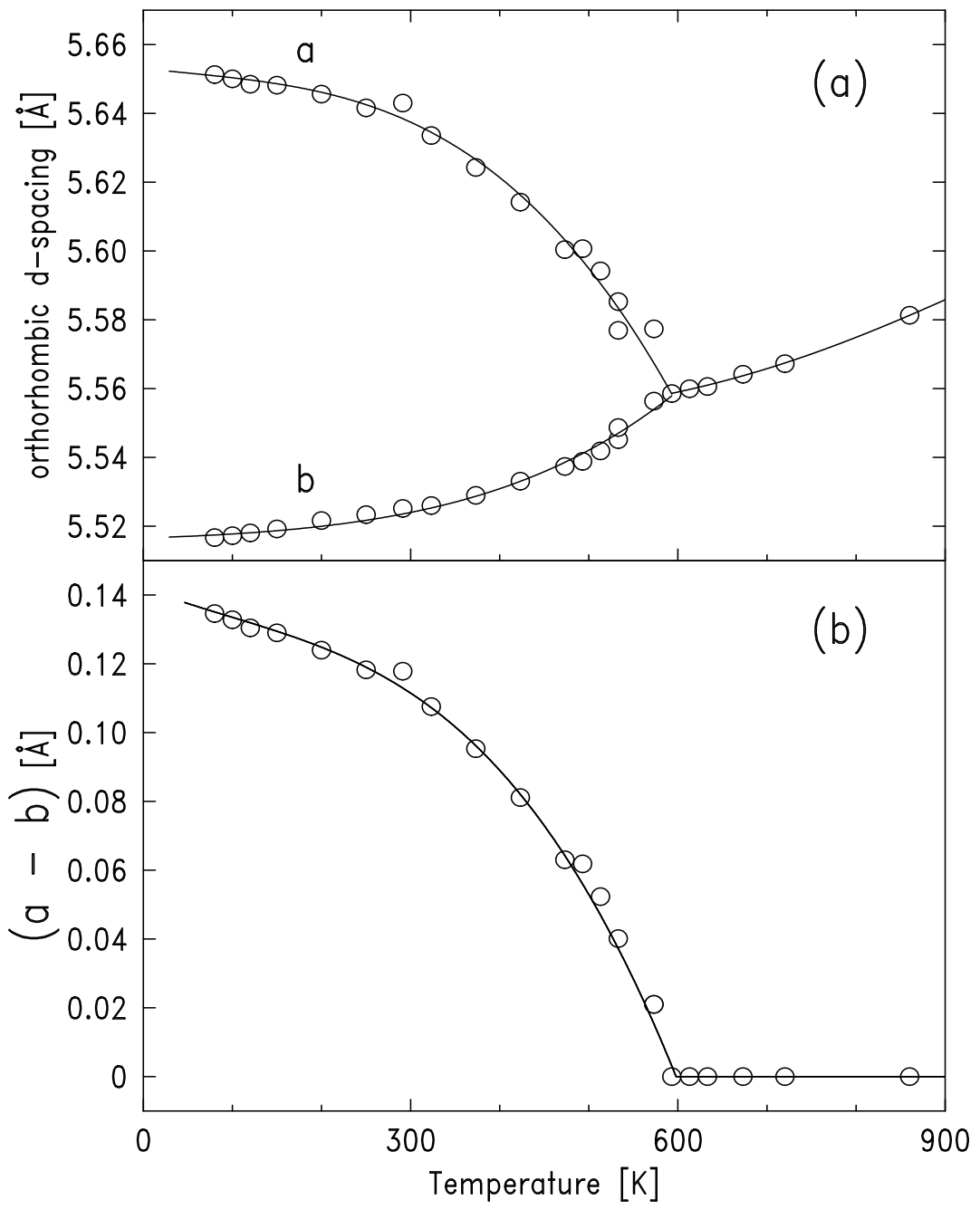


FIG. 2: Song et al.

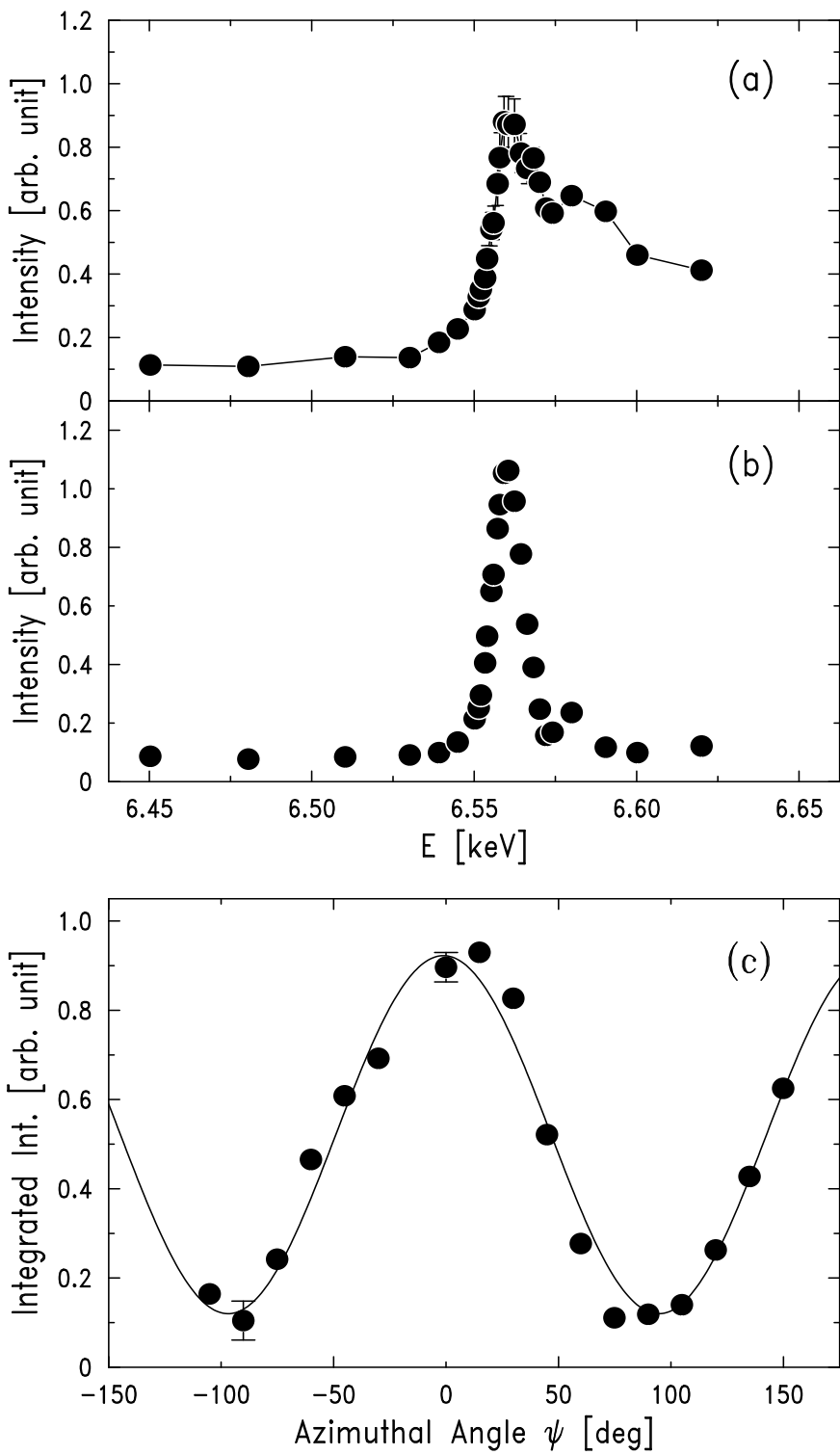


FIG. 3: Song et al.

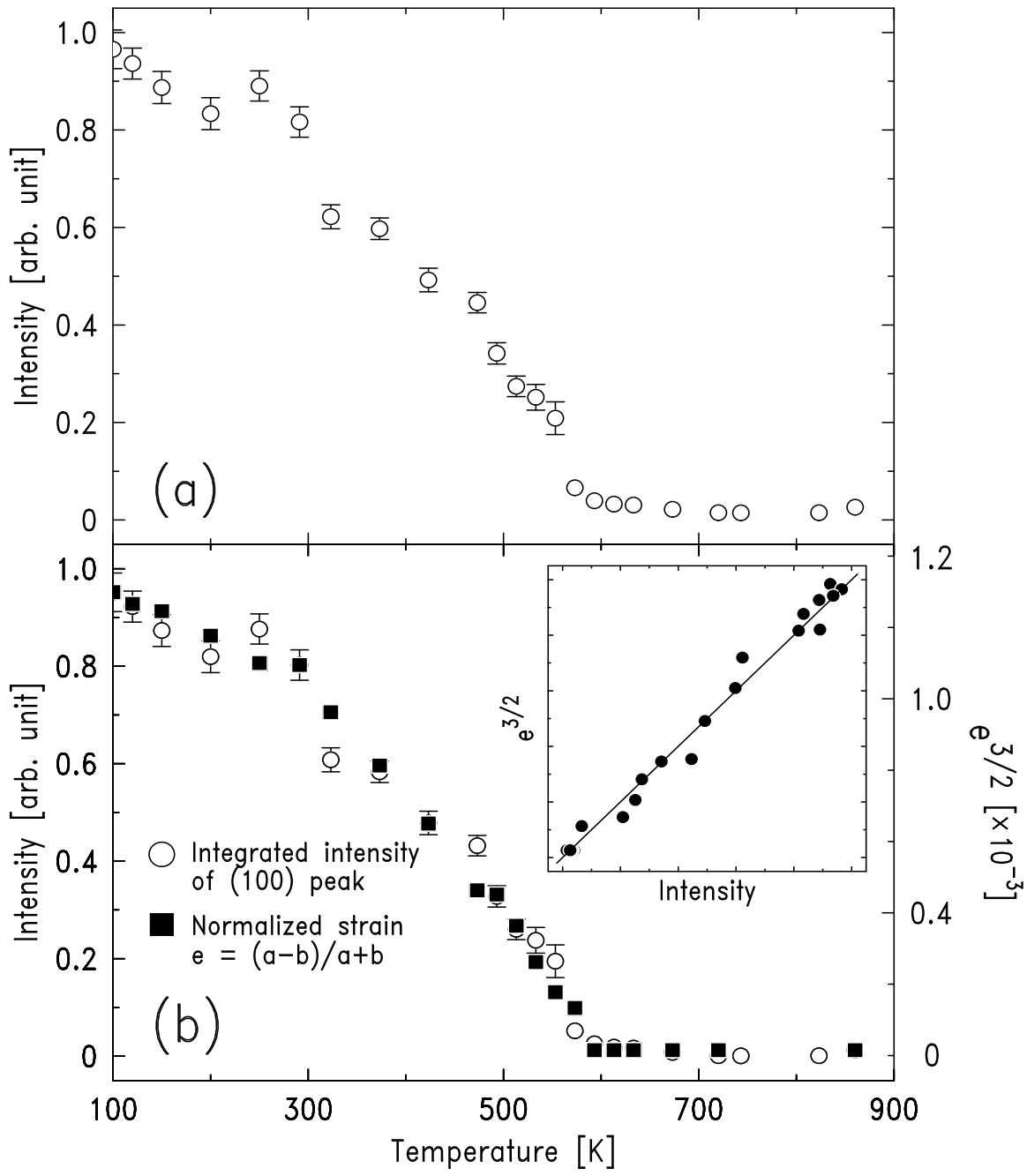


FIG. 4: Song et al.